JOURNAL OF CHEMICAL INFORMATION AND MODELING

Article

pubs.acs.org/jcim

Targeting Histidine Side Chains in Molecular Design through Nitrogen−Halogen Bonds

Andreas Lange,[†] Markus O. Zimmermann,[†] Rainer Wilcken,[†] Stefan Zahn,[‡] and Frank M. Boeckler*[,†]

[†]Laboratory for Molecular Design and Pharmaceutical Biophysics, Department of Pharmaceutical and Medicinal Chemistry, Institute of Pharmacy, Eberhard-Karls-University Tübingen, Auf der Morgenstelle 8, 72076 Tübingen, Germany

[‡]Wilhelm-Ostwald-Institut für Physikalische und Theoretische Chemie, Universität Leipzig, Linnéstraβe 2, 04103 Leipzig, Germany

Supporting Information

ABSTRACT: Halogen bonds are directional noncovalent interactions that can be used to target electron donors in a protein binding site. In this study, we employ quantum chemical calculations to explore halogen···nitrogen contacts involving histidine side chains. We characterize the energetics on the MP2 level of theory using SCS-MP2 and CCSD(T)/CBS as reference calculations and elucidate their energy profile in suboptimal geometries. We derive simple rules allowing medicinal chemists and chemical biologists to easily determine preferred areas of interaction in a binding site and exploit them for scaffold decoration and design. Our work shows that nitrogen−halogen bonds are valuable interactions that are this far underexploited in patent applications, lead structure, and clinical candidate selection. We highlight their potential to increase binding affinities and suggest that they can significantly contribute to inducing and tuning subtype selectivities.

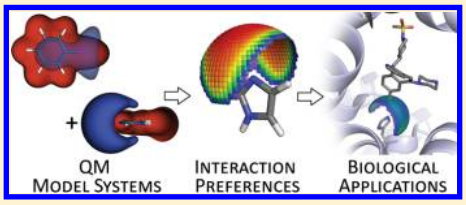

INTRODUCTION

Structure-based molecular design is facilitated by profound insights into molecular recognition. In recent years, established types of protein−ligand interactions, such as hydrogen bonds or hydrophobic contacts, have been complemented by other favorable interactions, such as weak hydrogen bonds, orthogonal multipolar interactions, halogen bonds, and other σ-hole interactions, $\pi-\pi$ contacts, cation$-\pi$ contacts, or CH$-\pi$ contacts.[1] However, awareness of this extended spectrum of interactions is not enough for its use in molecular design. Thorough studies evaluating the energy profile of such interactions in optimal and suboptimal geometries can guide their application to medicinal chemistry and chemical biology.[2−4]

Halogen bonding increasingly attracts attention. It is defined as an attractive contact of the type R−X···D−R′, where the electron pair acceptor atom X represents chlorine, bromine, or iodine and the electron pair donor atom D can be any kind of Lewis base. Although it is a well-known paradigm in materials sciences,[5,6] its occurrence in biological systems has been observed more recently, e.g., through statistical PDB evaluations.[7] The driving force of the interaction can be explained within the σ-hole concept: in elongation of the R−X bond, the halogen atoms possess a characteristic positive molecular electrostatic potential due to a deficiency in electron density in the outer lobe of the p_z orbital (where z is chosen as the R−X bond axis).[8−10] It should be noted that this concept has also been extended to other elements with potential relevance in biological systems.[11−13]

Several quantum chemical studies using small model systems have been performed to characterize nature and strength of halogen bonds.[2,3,14,15] In addition, protein−ligand complexes involving halogen bonds have been assessed by semiempirical QM and QM/MM calculations.[16−19] Recently, the OPLS-AA and OPLS/CM1A force fields have been enhanced to recognize attractive contributions in protein−ligand complexes based on halogen bonding.[20] In addition, the AMBER small molecule force field (GAFF) has been modified to include a molecular mechanical explicit σ-hole (ESH) as a massless point charge.[21] Halogen bonding has been compared to hydrogen bonding, and their similarities and differences have been discussed.[22−25] Several benchmarking studies have been carried out to elucidate preferred quantum chemical methods for describing halogen bonds.[26,27] While most halogen bonds that were observed in crystal structures of protein−ligand complexes were usually not designed,[28,29] several recent studies report the application of halogen bonding by fragment-based screening of HEFLibs (halogen-enriched fragment libraries)[30] or molecular design.[31−33]

In a recent analysis of ligand−protein halogen bond contacts based on the PDB,[17] predominantly two types of halogen bonds were found, contacts involving backbone carbonyl moieties (53%) as well as halogen···π contacts (33%). In contrast, interactions with sulfur or nitrogen were found less frequently (5% S, 9% N). Despite these numbers, nitrogen−halogen bonds certainly are favorable interactions. Because halogen bonds observed in the PDB are rarely designed, but typically found by crystallographic analysis, it is quite possible that halogen−nitrogen contacts are merely underrepresented. The statistics of the PDB analysis, thus, have to be amended taking the frequency of nitrogen (as a Lewis base) versus the

Received: July 23, 2013
Published: October 15, 2013

dx.doi.org/10.1021/ci4004305 | J. Chem. Inf. Model. 2013, 53, 3178−3189

ubiquitously present carbonyl oxygen into account. In this study, we provide evidence that targeting nitrogen as a Lewis base in histidine by halogen bonding has good potential for improving affinity and selectivity of a compound in molecular design. Thus, halogen bonding nicely complements the various other interactions shown by histidine (e.g., donating or accepting hydrogen bonds, charged interactions, metal complexation, and $\pi-\pi$-interactions).

In this work, we use quantum chemical calculations at the DFT-D, MP2 and CCSD(T) level in combination with a large basis set to characterize the interaction strengths between ligand model systems and two different molecular representations of histidine. We have used our best endeavors to ensure that the obtained interaction geometries merely represent the halogen bond contact, while avoiding additional secondary interactions. From our model calculations, we deduce simple rules how to best address the nitrogen atoms in histidine through halogen bonding and elucidate the impact of deviations from ideal binding geometries on overall complex formation energies. Finally, we apply our visualizations of the favorable areas of interaction within a binding site and demonstrate that our model calculations are in good agreement with existing crystal structures of farnesyl transferase in complex with chlorine and bromine containing benzo[5,6]cyclohepta[1,2-*b*]pyridine derivatives.[34,35]

RESULTS

Structure and Energetics of the Nitrogen−Halogen Bond. For studying the behavior of halogen bonds involving histidine, we used two different model systems for their representation: (i) imidazole (HIS1), the smallest reasonable system, and (ii) the full N^{δ}-protonated amino acid with a capped backbone using an acetyl group at the N-terminus and a N-methyl amid at the C-terminus (HIS2) (Figure 1). To avoid secondary interactions and biologically unreasonable backbone conformations, we restricted both backbone angles in all optimizations of HIS2 to an α-helical backbone conformation with $\varphi = -57.6°$ and $\psi = -47.5°$. The side chain conformation of HIS2 is trans. The dihedral angles $\chi_1(N-C^{\alpha}-C^{\beta}-C^{\gamma}) = -158.8°$ and $\chi_2(C^{\alpha}-C^{\beta}-C^{\gamma}-N^{\delta}) = -60.3°$ were fixed to avoid secondary interactions. Additionally, the angle $\delta(C^{\beta}-C^{\gamma}-N^{\delta}-H)$ was fixed to avoid deviations from a planar position of the hydrogen with respect to the imidazole ring. In contrast to HIS2, HIS1 is small enough to allow an extensive number of calculations at the MP2 level, as well as reference calculations at the CCSD(T) level of theory, while still representing the essential chemical substructure of histidine for studying the nitrogen···halogen interaction. In medicinal chemistry, aromatic or heteroaromatic scaffolds are commonly decorated with halogens (particularly chlorine, increasingly bromine, still rarely iodine), while aliphatic halogens are usually omitted, because of their reactivity. Therefore, we employ the three minimalistic halobenzenes (iodobenzene, bromobenzene, and chlorobenzene) as ligand models. In order to put the halogen bond strengths into context, we also use benzene and phenol as ligand models, representing weak and moderately strong hydrogen bonding to the nitrogen atom. Figure 2 shows the adduct formation reaction for the halobenzenes and HIS1. The molecular electrostatic potentials for both binding partners emphasize that the σ-hole is the driving force for binding as an electron acceptor to the negatively charged potential generated by the nitrogen in the imidazole ring.

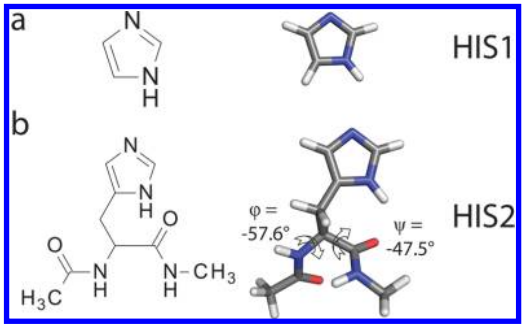

Figure 1. Histidine model systems: HIS1 (a) and HIS2 (b), represented as structural formulas and stick models (optimized geometries).

For all three halobenzenes, we obtained halogen-bonded complexes with HIS1 at the MP2/TZVPP level. We differentiated between two adduct conformations: the halobenzene ligands were placed (A) orthogonal to HIS1 (with respect to the planes of both aromatic rings) to avoid potential secondary interactions and (B) parallel to HIS1. Interaction energies for both conformations were calculated as adduct formation of the halogen-bonded complex from the isolated halobenzene and the histidine model system and the results of A can be seen in Table 1 and Figure 4 and for B in the Supporting Information (Table S1 and Figure S1). For orthogonal and parallel ligand conformations we obtained almost identical interaction energies. For further in-depth discussion of the complex formation energies, we only considered the orthogonal conformation to minimize the risk of potential secondary interactions, particularly when investigating deviations from the optimal geometries. The iodobenzene complex showed the strongest interaction energy with (−16.0 kJ/mol). We obtained weaker interaction energies for bromobenzene and chlorobenzene (−8.9 and −4.3 kJ/mol, respectively). These results are in agreement with the previously reported order of halogen-bond strengths in the literature.[10,25] This is correlated with the size of the σ-hole, visualized in Figure 3 by the extent of the positive

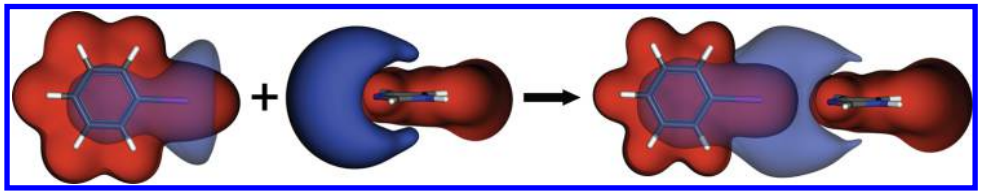

Figure 2. Adduct formation reaction of the iodobenzene···HIS1 complex displaying their molecular electrostatic potentials (ESP) calculated at MP2/TZVPP level. Positive ESP surfaces isocontoured at an energy of 0.02 au are colored in red indicating areas of favorable interactions with negative charges. Negative ESP surfaces isocontoured at an energy of −0.02 (or −0.01 for iodobenzene) are colored in blue indicating areas of attractive contacts with positive charges in the interacting molecule. All pictures were prepared with MOLCAD.[66,67]

dx.doi.org/10.1021/ci4004305 | J. Chem. Inf. Model. 2013, 53, 3178−3189

Table 1. Interaction Energies (kJ/mol) for Halogen-Bonded Model Complexes of the Small Histidine Model System HIS1 with an Orthogonal Orientation of the Ring Planes toward Each[a]

complex	ΔE [kJ/mol]	method	$d_{N5\text{-}X6/H6}$ (% vdW[b])	$\alpha_{C4-N5-X6/H6}$	$\delta_{N3-C4-N5-X6/H6}$	$\alpha_{N5\text{-}X6/H6-C7/O7}$
$C_6H_5I\cdots$HIS1	−16.0 (−20.4)	MP2/TZVPP	303 pm (84.4%)	132.8°	−177.6°	178.3°
$C_6H_5Br\cdots$HIS1	−8.9 (−11.3)	MP2/TZVPP	307 pm (89.4%)	133.1°	−177.9°	178.4°
$C_6H_5Cl\cdots$HIS1	−4.3 (−6.3)	MP2/TZVPP	314 pm (95.1%)	133.5°	−178.1°	178.9°
$C_6H_6\cdots$HIS1	−9.2 (−11.4)	MP2/TZVPP	243 pm (91.7%)	128.1°	176.9°	178.5°
$C_6H_5OH\cdots$HIS1	−43.2 (−48.9)	MP2/TZVPP	181 pm (68.3%)	113.0°	177.2°	167.0°
$C_6H_5I\cdots$HIS1	−13.1 (−17.1)	SCS-MP2/TZVPP	309 pm (86.1%)	132.9°	−177.8°	178.0°
$C_6H_5I\cdots$HIS1	−17.6	CCSD(T)/ CBS[c]	309 pm (86.1%)	132.8°	−177.8°	178.0°

[a]Interaction energies for complex formation with benzene and phenol (H···N contacts) are given for comparison. Energies were corrected for BSSE using the counterpoise correction of Boys and Bernardi.[49] Uncorrected energies are given in brackets. [b]Percentage of the sum of the van der Waals radii of the two atoms directly involved in bonding. [c]CCSD(T) calculations were performed on the SCS-MP2/TZVPP minimum geometry and a basis set extrapolation scheme was employed (see Methods).

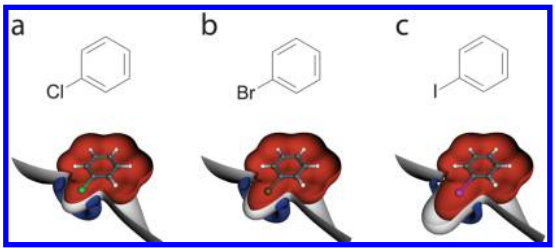

Figure 3. Structures and ESP isosurfaces of halobenzenes (MP2/TZVPP). Negative ESP isosurfaces at an energy of −0.012 au are colored in dark blue and positive ESP isosurfaces at 0.012 au are colored in red. The isosurfaces at 0.000 au, indicating the boundaries for the transition between negative and positive ESPs, are shown as gray surfaces. From chlorobenzene (a), to bromobenzene (b), and iodobenzene (c), the σ-hole (positive charge) on the halogen opposite of the R−X bond increases, while the belt of negative electrostatic potential becomes less pronounced. All pictures were prepared with MOLCAD.[66,67]

molecular electrostatic potential (red) piercing through the ring of negative molecular electrostatic potential (blue) in elongation of the carbon−halogen bond.[4]

With 303 pm (which is less than 85% of the sum of the van der Waals radii), the iodine···nitrogen contact is the shortest indicating a rather favorable interaction. The calculated equilibrium distances (Table 1) of all three complexes were found to be quite similar. Interestingly, the distance increases from iodobenzene (303 pm) to bromobenzene (307 pm) and chlorobenzene (314 pm). The decreasing bond distance from chlorine to iodine can be explained by the increasing σ-hole size and increasing polarizability of the halogen atom. We obtained similar results (Supporting Information Table S2), when using common density functionals (such as BP86, TPSS, BLYP, and B3LYP) with the second version (D2) of the empirical dispersion correction proposed by Grimme.[36]

Additionally, we compare these halogen bonds to a weak hydrogen bond formed by benzene and HIS1, as well as a moderately strong hydrogen bond between phenol and the HIS1 system at the MP2/TZVPP level. As expected, the interaction distance of the benzene···HIS1 complex was found to be much shorter than the calculated distance of the halobenzene···HIS1 complexes (243 vs 303 pm, H vs I). However, this distance represents 91.7% of the sum of the van der Waals radii, which is a similar percentage as found for chlorobenzene (95.1%) and bromobenzene (89.4%), but significantly larger percentage than iodobenzene (84.4%). The energy of the benzene−histidine adduct formation was −9.2 kJ/mol, whereas phenol formed a complex with HIS1 yielding the most favorable interaction energy of all investigated model systems (−43.2 kJ/mol).

As MP2 is known to partially exaggerate the quality of the interaction,[26,27] we have compared the geometry and energy obtained for iodobenzene···HIS1 at MP2/TZVPP with SCS-MP2/TZVPP and CCSD(T) using the complete basis set extrapolation (CBS) proposed by Halkier et al.[37] Except for a slight elongation in the iodine···nitrogen distance by 6 pm, the geometry is virtually identical when using SCS-MP2 instead of MP2 (Table 1). The bond angle $\alpha_{C4-N5-X6}$ and the dihedral angle $\delta_{N3-C4-N5-X6}$ change only by 0.1°, while the bond angle $\alpha_{N5-I6/H6-C7}$ decreases by 0.3°. The BSSE corrected SCS-MP2 adduct formation energy is −13.1 kJ/mol, while the non-corrected energy is −17.1 kJ/mol. Both SCS-MP2 energies are roughly 3 kJ/mol smaller than the corresponding MP2 values. However, applying the CCSD(T) level of theory together with the complete basis set extrapolation, the BSSE-corrected adduct formation energy is found to be −17.6 kJ/mol. As a pragmatic way to handle the multiplicity of calculations needed to describe the geometry dependence of the interaction, we have used the uncorrected MP2 energies as a metric for relative comparison of interaction energies, being aware that the actual BSSE-corrected high-level energies should be about 15% below the presented values.

We also have compared the halogen···nitrogen contact based on the histidine model system HIS1 to halogen···oxygen and halogen···sulfur contacts employing similarly small model systems of the backbone carbonyl (*N*-methylacetamide)[3] and of the methionine side chain (dimethylsulfide).[2] It should be noted that the result of this comparison is similar for MP2/TZVPP energies and for BSSE-corrected MP2/TZVPP energies. For iodine, there is a very small preference of the iodine···nitrogen (BSSE-corrected MP2/TZVPP energy: −16.0 kJ/mol) over the iodine···sulfur (−15.2 kJ/mol)[2] and the iodine···oxygen contact (−14.2 kJ/mol).[3] In contrast, bromine seems to benefit slightly more from the sulfur contact (−10.7 kJ/mol)[2] than from contacts to oxygen (−9.0 kJ/mol)[3] or nitrogen (−8.9 kJ/mol). Chlorine shows a higher preference for sulfur (−7.8 kJ/mol)[2] than for oxygen (−5.6 kJ/mol)[3] than for nitrogen (−4.3 kJ/mol). In summary, the interaction energy clearly is less dependent on the type of Lewis base than on the size of the σ-hole of the halogen.

For estimating trends in the desolvation penalties for the formation of halogen bonds in comparison to weak and moderately strong hydrogen bonds, we calculated the exchange of ligand-bound water by ligand-bound histidine (Figure 4).

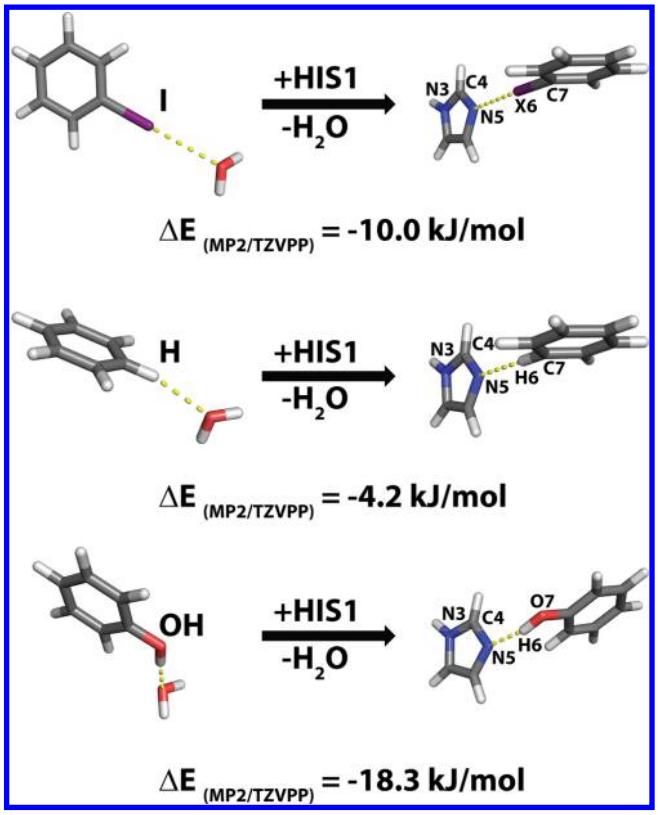

Figure 4. Reactions representing ligand desolvation. (a–c) Exchange of water from iodobenzene···water (a), benzene···water (b), and phenol···water (c) complexes by imidazole (HIS1) and corresponding reaction energies (kJ/mol) at MP2/TZVPP level. These three model systems represent (a) halogen bonds and (b) weak and (c) moderately strong hydrogen bonds. Relevant atom labels, which are used for defining distances, angles, and dihedrals, are shown in the complexes.

The complex formation energy is decreased from −20.4 kJ/mol (adduct formation reaction) to −10.0 kJ/mol (adduct formation by displacement of one water molecule) when the iodine···nitrogen contact is formed. The loss for the weak hydrogen bond is less pronounced (adduct formation −11.4 kJ/mol water displacement −4.2 kJ/mol). In contrast, the complex formation energy for a moderately strong hydrogen bond between phenol and HIS1 is dramatically reduced from −48.9 to −18.3 kJ/mol. Of course, this one-molecule approach to model solvation is rather simplistic, but it demonstrates that halogen bonds can approach the interaction quality of a moderately strong hydrogen bond when desolvation effects are taken into account. For comparison, we have additionally calculated COSMO-corrected interaction energies[38] (Supporting Information Table S4) by employing the continuum solvation model for various permittivity values reflecting protein environment (ε = 4) to water environment (ε = 78.4). For iodobenzene, a similarly impaired adduct formation energy of −12.6 kJ/mol is retrieved for the water environment. However, the adduct formation energy of benzene is more strongly reduced to −1.8 kJ/mol, while the adduct formation energy of phenol is preserved significantly better (−34.7 kJ/mol). In addition, we have calculated the solvation enthalpy ΔG_{solv} using COSMO-RS[39] with the parameter set optimized for BP86(RI)/TZVP (Supporting Information Table S5). This model indicates an increase in the interaction energy of −8.8 kJ/mol for iodobenzene, of −9.9 kJ/mol for bromobenzene, and of −11.2 kJ/mol for chlorobenzene compared to the gas phase, whereas benzene is predicted to gain less (−7.4 kJ/mol) and phenol should loose slightly (+2.3 kJ/mol) in interaction energy. As a result, the interaction energy of the halogen bonds is −24.8 kJ/mol (iodobenzene), −18.8 kJ/mol (bromobenzene), and −15.5 kJ/mol (chlorobenzene) in water. Interestingly, in both COSMO and COSMO-RS calculations the gap between the interaction energies of the best halogen bond (formed by iodobenzene) and the hydrogen bond (formed by phenol) remains larger than in the explicit one water-exchange model.

Finally, we performed geometry optimizations on the larger histidine model system HIS2. Compared to HIS1, the interaction energies with HIS2 are marginally higher (Table 2). While the geometries of iodobenzene and bromobenzene remain virtually unchanged, chlorobenzene showed a small change in the geometry of the larger systems as compared to the smaller one (Supporting Information Table S3 and Figure S2). In summary, halogen bonds on histidine can be favorable, especially those involving Br···N and I···N contacts. On the basis of the more frequent occurrence of chlorine in small molecular complexes in the PDB, most experimentally determined halogen bonds toward histidine in the PDB are formed by ligands containing chloro substituents. According to data presented herein, we suggest that exchange of these chlorines by bromine or iodine is feasible and could often be energetically favorable. Of course, other favorable types of contacts between halogens and histidine can be formed as well, e.g. interactions between a protonated histidine and the equatorial belt of electron density around the halogen (visualized as negative molecular electrostatic potentials in Figure 3).

Distance Dependencies of Halogen Bonds. In crystal structures, such optimal geometries as described above are rarely observed due to a complex network of multiple competing, additive, or cooperative primary and secondary interactions involved in ligand binding. For this reason, we investigate the influence of nonideal bond distances on complex formation energy. Starting from the MP2/TZVPP minimum structures, we perform distance scans along the X···N axis (Figure 5). The scans are carried out as single point MP2/TZVPP calculations using the histidine model HIS1, because

Table 2. Interaction Energies (kJ/mol) for Halogen-Bonded Model Complexes of the Large Histidine Model System HIS2 with an Orthogonal Orientation of the Ring Planes toward Each[a]

complex	ΔE [kJ/mol]	method	$d_{N5\text{-}X6/H6}$ (% vdW[b])	$\alpha_{C4-N5-X6/H6}$	$\delta_{N3-C4-N5-X6/H6}$	$\alpha_{N5-X6/H6-C7/O7}$
C_6H_5I···HIS2	−17.2 (−22.1)	MP2/TZVPP	302 pm (84.1%)	146.0°	178.3°	174.0°
C_6H_5Br···HIS2	−10.2 (−12.8)	MP2/TZVPP	307 pm (89.4%)	154.4°	179.9°	171.4°
C_6H_5Cl···HIS2	−6.1 (−8.4)	MP2/TZVPP	314 pm (95.1%)	162.7°	−179.1°	167.4°

[a]Energies were corrected for BSSE using the counterpoise correction of Boys and Bernardi.[49] Uncorrected energies are given in brackets. [b]Percentage of the sum of the van der Waals radii of the two atoms directly involved in bonding.

dx.doi.org/10.1021/ci4004305 | J. Chem. Inf. Model. 2013, 53, 3178–3189

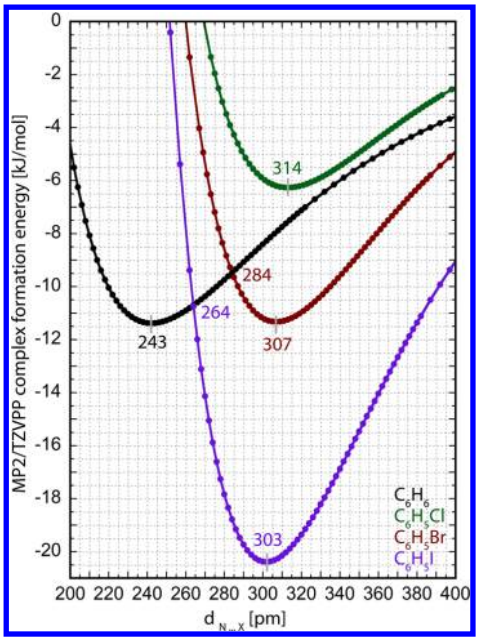

Figure 5. Distance scan plots for the three halobenzene···HIS1 complexes and benzene···HIS1 as comparison. The distance of X···N (H···N) is plotted against the complex formation energy of iodobenzene (purple), bromobenzene (brown), chlorobenzene (green), and benzene (black) complexes at the MP2/TZVPP level of theory.

the two histidine systems show quite similar behavior in terms of energetics. A comparison of distance scans of the small system (HIS1) versus the large system (HIS2) can be found in the Supporting Information (Figure S3). We additionally performed a distance scan using SCS-MP2 for the HIS1 system and found the MP2 and the SCS-MP2 curve very well matched with a small increase in the optimal distances by 7 pm and a scaling factor of 0.83 for the SCS-MP2 curve (Figure S3a). In addition to the MP2 method, we also carry out the distance scans employing four widely used density functionals (BP86-D, BLYP-D, B3LYP-D, and TPSS-D, Supporting Information Figure S4). TPSS-D shows the best agreement with the MP2 data while being much less computationally expensive.

In rational drug design, introduction of additional substituents such as halogen atoms into a lead structure is usually performed to gain higher affinity. Halogen bonds certainly can be favorable interactions, however, the H···N contact of an undecorated scaffold (e.g., benzene) can be favorable as well. Thus, we have to compare the complex formation energy of the halobenzene−histidine complexes with the benzene−histidine complex at the ideal halogen bond distance. This distance is very similar for all three halogenated complexes (303, 307, and 314 pm for I, Br, and Cl at MP2/TZVPP level). Figure 5 shows the distance dependence of the complex formation energies. At 303 pm, the complex formation energy for benzene is ΔE(MP2/TZVPP) = −8.2 kJ/mol (Table 3). Consequently, a net gain of approximately 12.2 kJ/mol should be possible for the substitution of hydrogen by iodine. For the substitution by bromine, a net gain of only roughly 3.4 kJ/mol can be expected, based on the complex formation energy for benzene of ΔE(MP2/TZVPP) = −7.9 kJ/mol at this distance. In contrast, substitution of hydrogen by chlorine seems not to be favorable at all, not even at the optimum distance for the halogen bond of 314 pm, where benzene still shows a complex formation energy of ΔE(MP2/TZVPP) = −7.5 kJ/mol.

Energetic Impact of σ-Hole Bond Directionality. As outlined before, the driving force of halogen bonding is the σ-hole, a region of positive charge on the chlorine, bromine, and iodine atom on the opposite side of its covalent bond (Figure 3). Consequently, halogen bonding is considered an electrostatic interaction similar to hydrogen bonding.[8,25] Riley et al. have suggested that halogen bonds may be driven by both electrostatic and dispersive forces, using symmetry-adapted perturbation theory.[14,40,41] Decomposition of interaction energies into dispersive and electrostatic/polarization contributions suggests that these contributions can be dependent on the particular interaction and binding situation. This includes the possibility that both might complement each other: if the positive electrostatic potential of the σ-hole becomes very high, the electrostatic character of the interaction is strengthened at the cost of the dispersive contribution, which is weakened based on the decreased polarizability of the halogen. The nature of the attractive force of halogen bonding, however, is not merely an academic dispute, but has practical consequences regarding the behavior of halogen bonds that need to be taken into account. A dispersion-driven interaction should tolerate deviations from the ideal bond angle $\alpha_{N5-X6-C7}$ rather well, while a purely electrostatic-driven interaction would be punished by quite significant penalties. Still, the polarizability of halogens is most likely rather anisotropic. For molecular design approaches, e.g. scaffold placement, knowledge about preferential directionality of an interaction certainly is of great importance. To evaluate the energy penalties of nonideal σ-hole bond angles, we have investigated the energetic impact of the σ-hole bond directionality. Starting from the optimized halobenzene···HIS1 complexes at MP2/TZVPP level, we successively varied the bond angle $\alpha_{N5-X6-C7}$ by steps of 5° in both directions and calculated single points for each step at MP2/TZVPP level. The results of the scans for all three halobenzenes are shown in Figure 6.

The optimal σ-hole angle is usually close to 180°. The scans show that for a halogen bond toward nitrogen (similar to halogen bond contacts with sulfur or carbonyl oxygen) changes from the optimal angle are strongly penalized. A deviation of 30° leads to a loss of interaction energy in the range of 50% to 60%. On the basis of this observation, we conclude that in this case halogen bonding is dominated by electrostatic forces, a

Table 3. Comparison of MP2/TZVPP Complex Formation Energies (kJ/mol) at Optimal Distances and at the Equilibrium Distance of Iodobenzene···HIS1

system	$d_{N5\cdots X6/H6}$ [pm]	$\Delta E_{MP2/TZVPP}$ at optimal distance	$\Delta E_{MP2/TZVPP}$ at 303 pm	intersection point with benzene based on distance
C_6H_5−**I**···HIS1	303	−20.4	−20.4	∼264 pm
C_6H_5−**Br**···HIS1	307	−11.3	−11.3	∼284 pm
C_6H_5−**Cl**···HIS1	314	−6.3	−6.1	N/A
C_6H_5−**H**···HIS1	243	−11.4	−8.2	N/A

dx.doi.org/10.1021/ci4004305 | J. Chem. Inf. Model. 2013, 53, 3178−3189

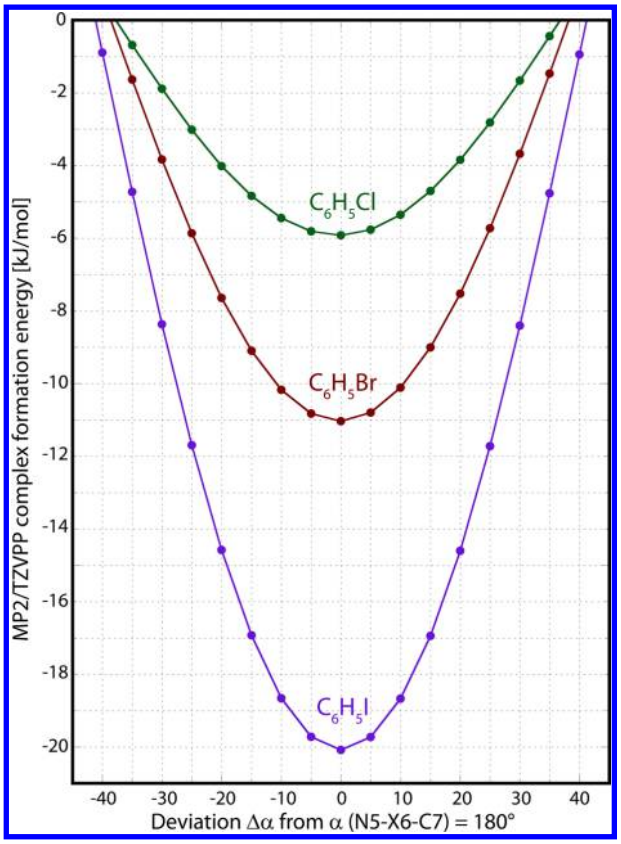

Figure 6. Impact of deviations from nearly 180° σ-hole angles $\alpha_{N5-X6-C7}$ for halobenzenes···HIS1 complexes. Energies calculated using MP2/TZVPP.

behavior being in accordance with other works.[8,10,24,25] Still it must be noted, that dispersion might play a role in cases of less positive σ-holes and highly anisotropic polarizabilities. To provide an estimate of the influence of dispersion, we have calculated the DFT-energies employing the common density functionals BP86, TPSS, BLYP, and B3LYP with and without the second version (D2) of the empirical dispersion correction proposed by Grimme.[36] For the iodobenzene complex, the dispersion correction contributes between 39% and 47% of the total dispersion corrected energy. For bromobenzene the dispersion seems to become the dominant contribution with ratios between 57% and 69%; whereas, for chlorobenzene dispersion seems to be the only favorable contribution to binding with ratios approaching 100%.

Dihedral Angle Variations — Spherical Scans. To facilitate applicability of halogen bonds in molecular design tools, we evaluated the preferential spatial orientation of the halobenzene···HIS1 halogen bond. We performed spherical scans around nitrogen N5 as the center, keeping the halobenzene at equilibrium distance at all times and varying both dihedral angles δ_1 (out-of-plane rotation) and δ_2 (in-plane rotation) that define the interaction geometry successively by 5° (Figure 7a). The obtained interaction spheres for iodobenzene···HIS1 from different perspectives are presented in Figure 7b and c. In this figure, every colored object represents one interaction geometry and its corresponding energy. The most favorable areas of interaction with adduct formation energies exceeding −16.5 kJ/mol form a spherical segment that reflects the accessibility of the free electron pair, as can be seen in the lower images of Figure 7b or c. This

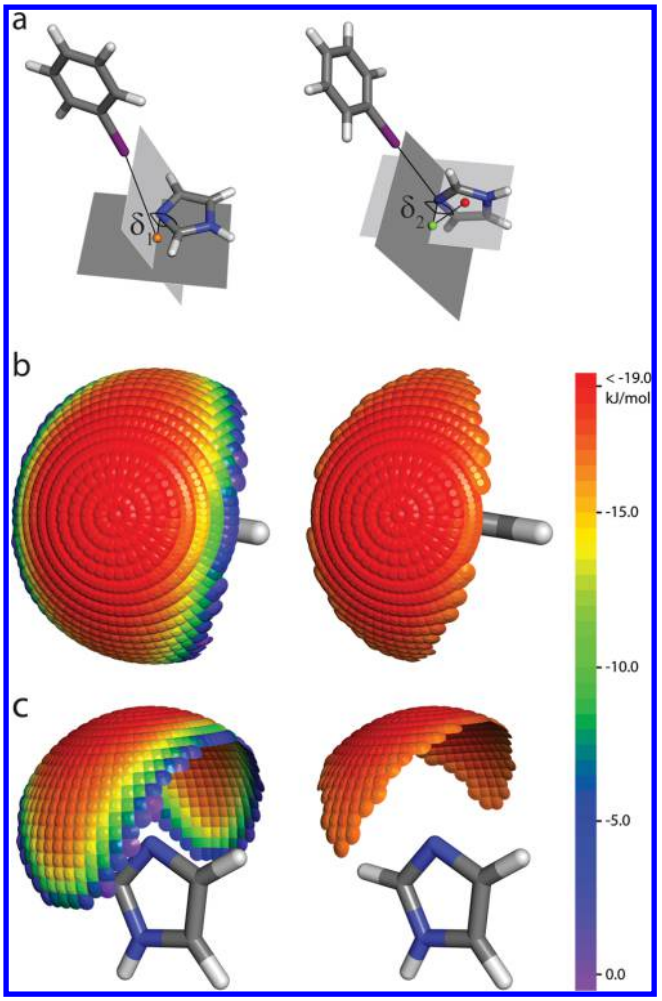

Figure 7. Spherical scans for iodobenzene. (a) Illustration of dihedral angle δ_1 (out-of-plane rotation) and δ_2 (in-plane rotation). δ_1 represents the rotation around an axis through the orange dummy point and atom N5, which is part of the imidazole plane and is oriented perpendicularly to the mirror plane of the imidazole fragment. δ_2 represents the rotation around an axis from the green dummy point to atom N5, which is oriented perpendicularly to the imidazole plane. (b) Spherical scan for the iodobenzene···HIS1 from the top. Favorable areas with energies better than −16.5 kJ/mol are shown in the picture to the right. (c) Sideview of the iodobenzene··· HIS1 sphere. Favorable areas with energies better than −16.5 kJ/mol are shown in the picture to the right.

hotspot of most favorable interaction energies extends in the out-of-plane direction to a δ_1 angle between −75° and +75°, whereas in the in-plane rotation only a δ_2 angle of −25° to +25° is tolerated. Beyond this interaction hotspot, the energy decreases rapidly based on clashes of iodobenzene with both hydrogens adjacent to N5 in the imidazole ring of HIS1. In summary, there is a substantial number of favorable interaction geometries. Although the interaction will naturally have a certain directionality, entropic penalties should be reduced by the number of iso-energetic interaction geometries and their impact on the flexibility of the halogen···nitrogen contact. Still, it is likely that histidine in a binding site would be ideally preoriented by other interactions (such as hydrogen bonds of the N^{δ} or $\pi-\pi$/cation$-\pi$ interactions of the imidazole), while the N^{ε} remains accessible for the halogen bond.

For bromobenzene, the preferred geometries are quite similar to iodobenzene, however, the interaction energies are

dx.doi.org/10.1021/ci4004305 | J. Chem. Inf. Model. 2013, 53, 3178−3189

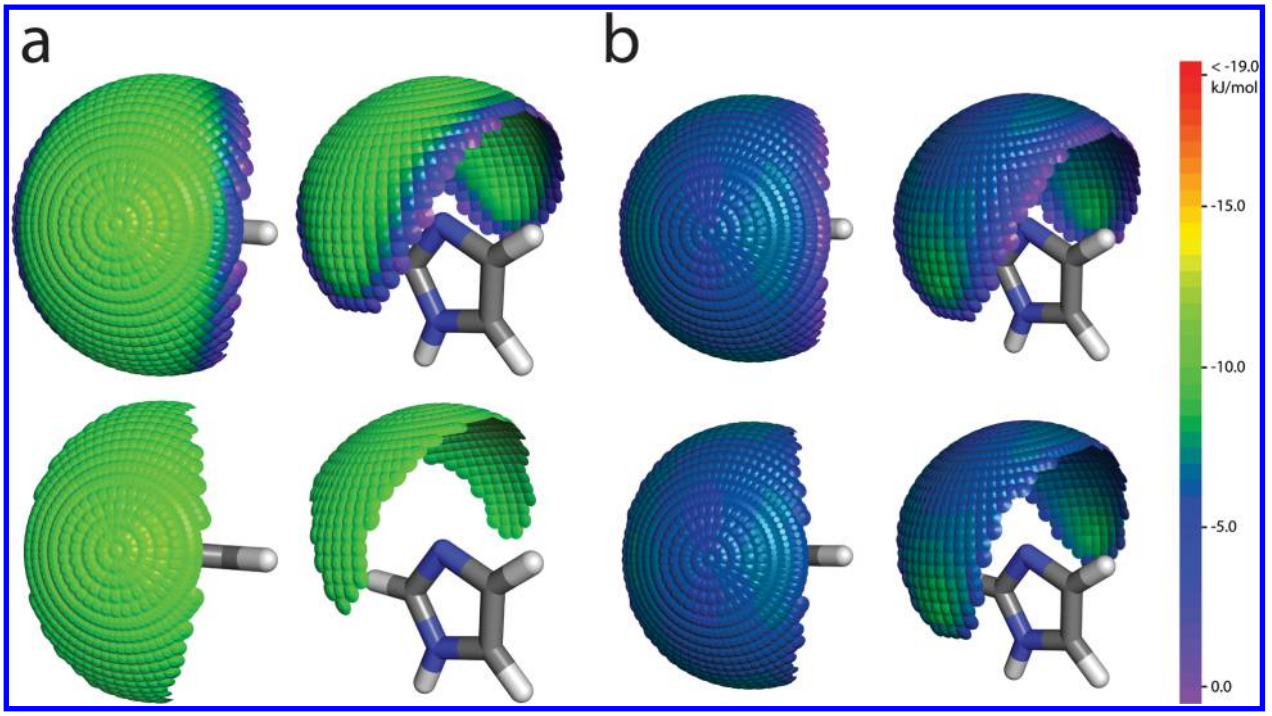

Figure 8. Spherical scans for bromobenzene and chlorobenzene. (a) Interaction energy sphere for the bromobenzene···HIS1 complex from top and from the side. Areas with energies better than −10 kJ/mol are shown below. (b) Interaction energy sphere for the chlorobenzene···HIS1 complex from top and from the side. Areas with energies better than −5 kJ/mol are shown below.

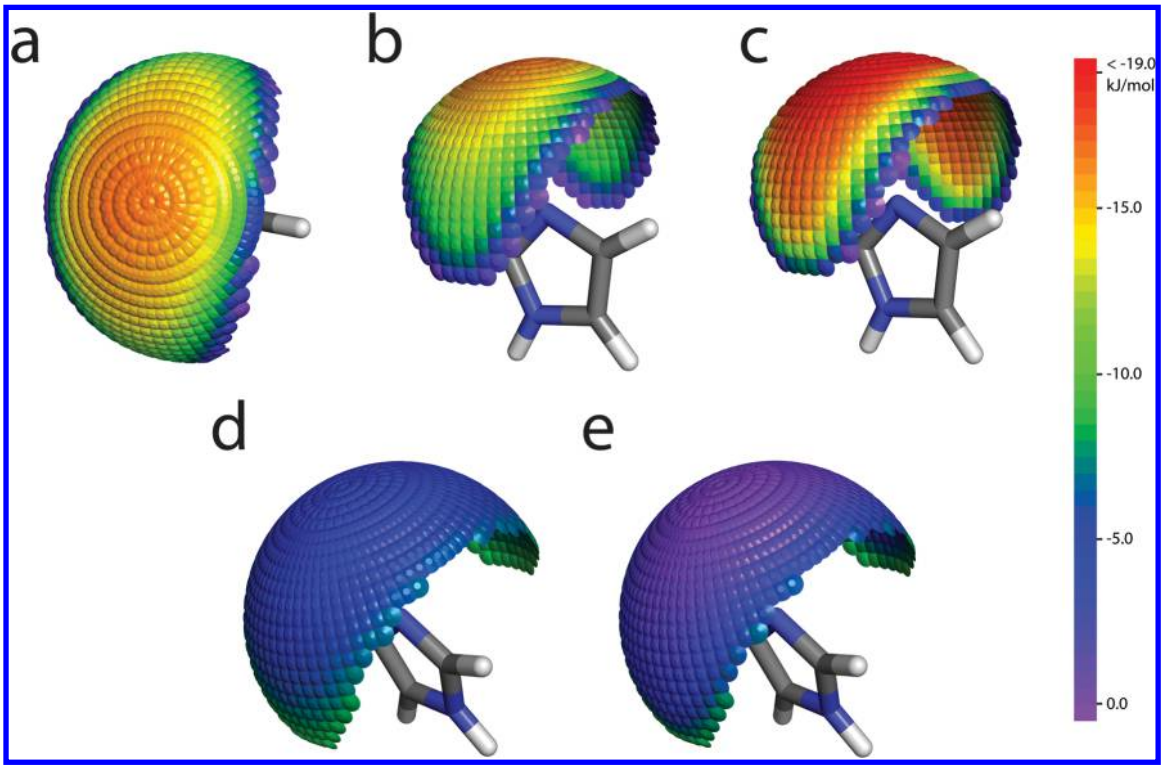

Figure 9. Comparison of the spherical scan of iodobenzene···HIS1 complex at MP2 and SCS-MP2 level. (a) + (b) Interaction sphere of iodobenzene···HIS1 at SCS-MP2 level shown from the top (a) and from the side (b). (c) Spherical scan of iodobenzene···HIS1 at MP2 level shown from the side. (d) Comparison between MP2 and SCS-MP2. Each spot represents the difference between MP2 energy minus SCS-MP2 energy (kJ/mol). (e) Comparison between MP2 and SCS-MP2 with a scaling factor of 0.83. Each spot represents the difference between MP2 energy multiplied by 0.83 minus SCS-MP2 energy (kJ/mol).

certainly lower (see Figure 8). For both the iodobenzene and bromobenzene, the best complex formation energy lies at an angle $\alpha_{1(C4-N5-X6)}$ of nearly 180° (see Table 1) and $\delta_{1(N3-C4-N5-X6)}$ of approximately 180°. In typically favorable orientations, iodobenzene always shows better interactions with the histidine model system than bromobenzene. The best

dx.doi.org/10.1021/ci4004305 | J. Chem. Inf. Model. 2013, 53, 3178−3189

complex formation energies for bromobenzene are found to amount to between −10.0 and −11.3 kJ/mol (Figure 8a). Remarkably, the favored orientation for chlorobenzene features an $\delta_{1(N3-C4-N5-X6)}$ angle of ±88° instead of 180° for the heavier halides, indicating a preference for an orientation almost perpendicular to the plane of the imidazole ring (Figure 8b). We suggest that this could be the result of additional attractive contacts in the transition between halogen···n-electron to halogen···π-electron interactions. We are currently extending our investigations to study these halogen···π contacts as well.

In a recent publication by Kozuch et al., different levels of theory were evaluated for their ability to correctly describe a diverse set of halogen bonds.[27] Although, of course, applicability of the results obtained for a diversity set of benchmarks on the particular halogen···nitrogen contact of our study can be limited, the superior performance of SCS-MP2 compared to MP2 should be considered. As discussed before, the energy−distance relationship obtained by MP2 calculations can be easily transformed by a small distance shift and a scaling factor to almost perfectly match the SCS-MP2 energies. Therefore, we have investigated whether a similar behavior is detectable for the spherical energies. We have recalculated our iodobenzene···HIS1 sphere on a SCS-MP2 level and compared it to the sphere obtained on the MP2 level (Figure 9). Most of the data points show a similar difference between MP2 and SCS-MP2: more than 67% show a difference between 3.5 to 5.0 kJ/mol and more than 75% between 3.5 and 5.5 kJ/mol. As visible in Figure 9d, the lowest differences are found in the more favored interaction geometries. When again scaling the MP2 energies by a factor of 0.83, 64% of the resulting energies (Figure 9e) deviated from the SCS-MP2 energies by less than 2 kJ/mol, 75% by less than 3 kJ/mol. Only interactions in particularly bad geometries (close to areas where the halobenzene clashes with the imidazole) are not decently reproduced by applying the scaling factor.

Finally, we also performed spherical scans for the large histidine model system (HIS2). These are presented in the Supporting Information (Figure S5), showing the same trends as for the small model system. It thus appears that the small model system (HIS1) is well suited to describe the isolated halogen bond void of secondary interactions.

DISCUSSION

We have proposed that halogen bonds addressing the nitrogen atom of a histidine side chain are favorable interactions that have so far been rather neglected in molecular and drug design. We have shown that all halobenzene model systems form complexes featuring very similar equilibrium distances (303−314 pm), a behavior also observed for other contacts.[2,3] This leads to the perception that chloro, bromo, and iodo moieties should be interchangeable as halogen bonding partners. Among the halobenzenes, iodobenzene had the strongest interaction energy with the used histidine model systems. The observed order of halogen bond strength (Cl < Br < I) is well in line with halogen bonds in other interactions.[4] Surprisingly, bromobenzene and benzene are energetically comparable at their individual optimal interaction distances of 307 and 243 pm, respectively. Through distance scans it is possible to check whether an introduction of a particular halogen into a benzene-based scaffold is reasonable. When evaluating only the direct interaction distance $d_{N5\cdots X6/H6}$, the interaction of chlorobenzene with histidine seems to be always inferior to benzene. It should be noted, however, that from the perspective of scaffold decoration, the energy profile with respect to the scaffold··· histidine distance $d_{N5\cdots C7}$ is crucial. The σ-hole scans confirm that halogen bonding is a highly directional interaction.

As we have recently shown, the favorable spherical angles of the halogen atom toward the carbonyl oxygen of the protein backbone can exist in a large variety of favorable spherical orientations.[3] Compared to the carbonyl oxygen moiety, the favorable spherical angles of a halogen toward the sulfur atom of methionine are rather restricted.[2] Halogen···nitrogen contacts involving histidine seem to be intermediate binding situations sharing only partial similarity with both other systems. In comparison to the carbonyl oxygen of the protein backbone, the nitrogen of the imidazole ring does not allow for as many similarly favorable interaction geometries but still significantly more than found at the restricted interaction hotspots of the sulfur atom in methionine (caused by the strongly anisotropic electron distribution around the sulfur atom). Obviously, clashes with the imidazole ring system as well as the presence of only one lone pair as an interaction partner are responsible for restricting the favored interaction areas. This result is true for both MP2 and SCS-MP2 spherical scans.

According to our results, a halogen bond between a ligand-bound chlorine and nitrogen as an electron donor in histidine is only a weak interaction. There are some PDB structures (slightly more than 200) showing halogen···nitrogen contacts; however, they rarely show good halogen bonding geometries. In the case of 2BED[34] (Figure 10a), one of the more suitable

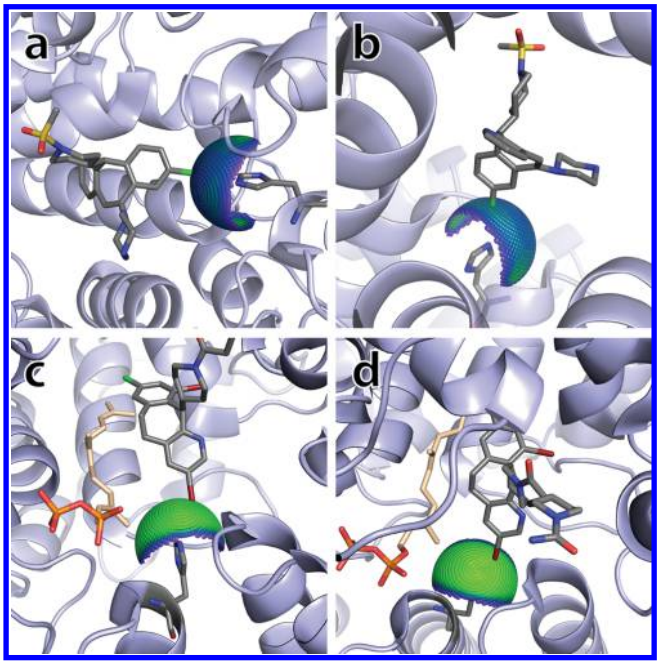

Figure 10. (a) + (b) Example for a chloroaryl···histidine halogen bond in the PDB (PDB code: 2BED, HIS201). The interaction sphere is projected onto the crystal structure of the protein−ligand complex. The ligand binds to His201 from an energetically favorable spherical position, as indicated in the projected spherical scan and shows a very reasonable σ-hole angle of 165°. Spectrum colors and associated energies are the same as shown in Figure 8. (c) + (d) Halogen bond for bromoaryl···histidine (PDB code: 1O5M, Chain A, HIS201). A quite acceptable σ-hole angle of 155°, as well as an energetically favorable spherical binding position is found for this ligand. Spectrum colors and associated energies are the same as shown in Figure 8

dx.doi.org/10.1021/ci4004305 | J. Chem. Inf. Model. 2013, 53, 3178−3189

examples, the σ-hole angle of 165° is still in the favorable region and the spherical orientation indicates an energetically favorable interaction, when projecting the computed interaction spheres (Figure 8) onto the interacting nitrogen atom (Figure 10a+b). Compared to bromine and iodine (together slightly more than 100 PDB structures), chlorine is a more commonly used halogen in drug-like ligands in the PDB. In 1O5M,[35] the σ-hole angle of 155° is acceptable and the bromine···nitrogen distance is very reasonable at 320 pm. The spherical orientation is well within the most favored region for bromine (Figure 10c and d). Comparing this tricyclic farnesyl protein transferase inhibitor (SCH 66336) with its enantiomer shows that alteration of the chirality at C11 of the 6,11-dihydro-5*H*-benzo[5,6]cyclohepta-[1,2-*b*]pyridine ring system from the (*R*)- to the (*S*)-isomer leads to an inverted orientation of the tricyclic ring in the binding site. As a consequence the 8-chloro instead of the 3-bromo substituent is presented to HIS201 and the tricyclic ring is rotated by approximately 12° to allow for the placement of bromine in position 10. The resulting complex of the (*S*)-enantiomer with farnesyl protein transferase (crystal structure shown in the work of Strickland et al.[35] but not published in the pdb) lacks a hydrogen bond toward the pyridine substructure and shows a significantly weaker halogen bond based on the chlorine−nitrogen contact and the worse geometry. These impairments in the binding interactions contribute to an ∼200-fold weaker inhibitory activity (IC_{50} values of 378 nM, instead of 1.9 nM for the (*R*)-enantiomer). Other structure activity relationship involving halogen−nitrogen contacts may become available by new tools for structure-based matched molecular pair analysis.[42]

Mapping the interaction spheres onto a histidine moiety in the binding site facilitates a quick and simple assessment of the accessibility of histidine side chains for the purpose of scaffold decoration in molecular design. Additionally, it provides insights that aid in the construction of compound libraries for virtual and biophysical screening campaigns. We have recently demonstrated this utilization by designing halogen-enriched fragment libraries (HEFLibs) for rescuing mutant p53.[30]

In commonly used molecular design tools, halogen bonds are presently not observed as attractive contributions to the binding energy. Thus, the results of this study will be useful for the development of design algorithms and scoring functions. A key element for medicinal chemistry and molecular design is an in-depth understanding of molecular interactions. Halogen bonding can enrich the drug discovery process and—despite its limitations—promote halogens from mere scaffold decorations to being part of the essential binding motif.

METHODS

DFT-D and MP2 Structure Optimizations. All DFT and MP2 calculations in this work were performed using the Turbomole 6.2 suite of programs.[43,44] The employed basis sets were of triple-ζ quality (def2-TZVPP).[45] MP2 calculations were done in combination with the resolution of identity (RI) technique[46−48] and the frozen core approximation. The frozen core orbitals were attributed by the default setting in Turbomole, by which all orbitals possessing energies below 3.0 au are considered core orbitals. The SCF convergence criterion was increased to 10^{-8} Hartree for all calculations. Interaction energies were counterpoise-corrected using the procedure of Boys and Bernardi[49] where indicated (see Table 1) in order to correct for basis set superposition errors (BSSEs). DFT calculations were performed using the RI approximation[50−52] with the BP86,[53,54] BLYP,[53,55] and TPSS[56] functionals. The RI approximation is not efficient for hybrid functionals and hence was not used in B3LYP[53,54,57] calculations. All functionals were augmented with the second version of Grimme's empirical dispersion correction,[36] which we have indicated by appending "-D" to their names (i.e., BP86-D, BLYP-D, TPSS-D, B3LYP-D).

CCSD(T) Calculations. The Turbomole-suite[43,44] was applied for the MP2 single point calculations with the cc-pVTZ and cc-pVQZ basis set.[58−60] Relativistic effects were considered by a relativistic pseudopotential.[60] These calculations were applied in combination with the RI-technique and the frozen core approximation.[47,61] The frozen core orbitals were attributed by the default settings of Turbomole which means all orbitals with an energy below 3.0 au were considered as core orbitals. CCSD(T) calculations were carried out with the cc-pVTZ[58−60] basis set employing the MOLPRO[62] program package. Relativistic effects for iodine were considered by a relativistic pseudopotential. All CCSD(T) and MP2 energies were counterpoise corrected with the procedure of Boys and Bernardi[49] in order to eliminate the basis set superposition errors (BSSEs).

The contribution of higher order correlation energy was determined by following scheme:

$$\Delta E_{CBS}^{CCSD(T)} = \Delta E_{CBS}^{MP2} + (\Delta E_{cc\text{-}pVTZ}^{CCSD(T)} - \Delta E_{cc\text{-}pVTZ}^{MP2}) \quad (1)$$

This is based on the assumption that the difference between the CCSD(T) and MP2 interaction energies ($\Delta E^{CCSD(T)} - \Delta E^{MP2}$) depends only slightly on the basis set and therefore can be determined with small or medium basis sets like cc-pVTZ.[63,64] ΔE_{CBS}^{MP2} is the MP2 energy at the complete basis set limit which was obtained by the extrapolation proposed by Halkier et al.:[37]

$$\Delta E_{CBS}^{MP2} = \frac{\Delta E_X^{MP2} X^3 - \Delta E_Y^{MP2} Y^3}{X^3 - Y^3} \quad (2)$$

where *X* and *Y* are the cardinal numbers of the cc-pVTZ and cc-pVQZ basis set, respectively.

Distance Scans. All distance scans were performed using the optimized MP2/TZVPP geometries as starting points. The bond distance $d_{X\cdots N}$ ($d_{H\cdots N}$ for benzene) were then elongated or shortened in 2 pm steps (5 pm further away from the minimum), with the rest of the ligand structure (halobenzene or benzene) transformed accordingly. For each step, single-point (SCF) calculations were performed using MP2/TZVPP. Additionally, DFT-D (TPSS-D, BP86-D, BLYP-D, and B3LYP-D) methods were used for the HIS1 model.

Spherical Scans. Input files were generated from the optimized MP2/TZVPP geometry. In order to generate a full sphere of input geometries for subsequent calculations, the optimized structure was transformed as follows:

The nitrogen atom was placed on the origin of the coordinate system and the entire complex was rotated until the halogen atom was positioned on the positive *x*-axis. Let α denote the angle of rotation counterclockwise around the *z*-axis and β denote the angle of rotation counterclockwise around the *x*-axis. α was gradually increased from 0° to 180° in steps of 5°. For each α-value, β was varied from 0° to 355° in steps of 5°, leading to a total number of 2664 halogen positions distributed on a sphere. The structure of the ligand was not altered during this transformation process. Calculations were done as single point (SCF) calculations using the MP2/TZVPP method.

dx.doi.org/10.1021/ci4004305 | J. Chem. Inf. Model. 2013, 53, 3178−3189

For visualization purposes, several Python scripts were written and executed in PyMOL.[65] Interaction energies were partitioned into bins and spectrum colors (red to blue to purple) were assigned. At the positions of the halogens small CONE objects with the appropriate coloring were generated.

■ ASSOCIATED CONTENT

Supporting Information

Comparison of MP2 and DFT-D methods for the complex formation energies and interaction geometries is given in Tables S1 and S2 for the parallel orientation and the orthogonal orientation of the halobenzene toward the histidine imidazole system (HIS1), respectively. For the orthogonal orientation of the halobenzene toward the larger HIS2 system, a similar comparison between MP2 and different DFT-D methods is summarized in Table S3. Interaction energies with COSMO correction are presented in Table S4. In Table S5, the difference of solvation enthalpies in water for complexes and their reactants (ΔG_{solv}) as calculated by the COSMO-RS approach is shown.

The adduct formation of the halobenzene···HIS1 complex, of benzene···HIS1 complex and of phenol···HIS1 complex in parallel orientation toward the imidazole ring, can be seen in Figure S1. The freely optimized structures for the three halobenzenes with the larger histidine model system HIS2 are represented in Figure S2. In Figure S3 a comparison of the small histidine model system HIS1 and the larger model system HIS2 as distance scan for iodobenzene (a), bromobenzene (b), and chlorobenzene (c) can be seen (MP2/TZVPP), as well as, the distance scan for iodobenzene···HIS1 at SCS-MP2/TZVPP level. Figure S4 presents a series of distance scans for HIS1 and the three halobenzenes comparing different DFT functionals with applied dispersion correction (TPSS-D(RI)/TZVPP, BP86-D(RI)/TZVPP, BLYP-D(RI)/TZVPP, and B3LYP-D/TZVPP). The spherical scan for iodobenzene···HIS2 (a), bromobenzene···HIS2 (b), and chlorobenzene···HIS2 (c) from the side and from the top can be seen in Figure S5. This material is available free of charge via the Internet at http://pubs.acs.org.

■ AUTHOR INFORMATION

Corresponding Author

*Phone: +4970712974567. Fax: +497071295637. E-mail: frank.boeckler@uni-tuebingen.de.

Notes

The authors declare no competing financial interest.

■ ACKNOWLEDGMENTS

High performance computing resources of the BW-Grid were kindly made available by the federal state of Baden-Wuerttemberg. S.Z. thanks the European Social Fond for financial support.

■ ABBREVIATIONS

BSSE, basis set superposition error; CCSD(T), coupled-cluster method with single, double and perturbative triple excitations; DFT, density functional theory; DFT-D, density functional theory augmented by an empirical dispersion correction; HEFLibs, halogen-enriched fragment libraries; HIS, histidine; MP2, second-order Møller−Plesset perturbation theory; OPLS-AA, optimized potentials for liquid simulations—all atoms; OPLS/CM1A, OPLS-AA force field incorporating polarized partial atomic charges obtained from the quantum mechanical CM1A procedure; PDB, Brookhaven Protein Data Bank; QM/MM, quantum mechanics/molecular mechanics; SCF, self-consistent field calculation; SCS-MP2, spin-component scaled second-order Møller−Plesset perturbation theory

■ REFERENCES

(1) Bissantz, C.; Kuhn, B.; Stahl, M. A medicinal chemist's guide to molecular interactions. *J. Med. Chem.* **2010**, *53* (14), 5061−5084.
(2) Wilcken, R.; Zimmermann, M. O.; Lange, A.; Zahn, S.; Kirchner, B.; Boeckler, F. M. Addressing Methionine in Molecular Design through Directed Sulfur−Halogen Bonds. *J. Chem. Theory Comput.* **2011**, *7* (7), 2307−2315.
(3) Wilcken, R.; Zimmermann, M.; Lange, A.; Zahn, S.; Boeckler, F. Using halogen bonds to address the protein backbone: a systematic evaluation. *J. Comput.-Aided Mol. Des.* **2012**, *26* (8), 935−945.
(4) Wilcken, R.; Zimmermann, M. O.; Lange, A.; Joerger, A. C.; Boeckler, F. M. Principles and Applications of Halogen Bonding in Medicinal Chemistry and Chemical Biology. *J. Med. Chem.* **2013**, *56* (4), 1363−1388.
(5) Hassel, O.; Hvoslef, J. The Structure of Bromine 1,4-Dioxanate. *Acta Chem. Scand.* **1954**, *8*, 873−873.
(6) Metrangolo, P.; Meyer, F.; Pilati, T.; Resnati, G.; Terraneo, G. Halogen Bonding in Supramolecular Chemistry. *Angew. Chem., Int. Ed.* **2008**, *47* (33), 6114−6127.
(7) Auffinger, P.; Hays, F. A.; Westhof, E.; Ho, P. S. Halogen bonds in biological molecules. *Proc. Natl. Acad. Sci. U.S.A.* **2004**, *101* (48), 16789−16794.
(8) Clark, T.; Hennemann, M.; Murray, J. S.; Politzer, P. Halogen bonding: the sigma-hole. *J. Mol. Model.* **2007**, *13* (2), 291−296.
(9) Murray, J. S.; Riley, K. E.; Politzer, P.; Clark, T. Directional Weak Intermolecular Interactions: sigma-Hole Bonding. *Aust. J. Chem.* **2010**, *63* (12), 1598−1607.
(10) Politzer, P.; Lane, P.; Concha, M. C.; Ma, Y. G.; Murray, J. S. An overview of halogen bonding. *J. Mol. Model.* **2007**, *13* (2), 305−311.
(11) Murray, J.; Lane, P.; Politzer, P. Expansion of the σ-hole concept. *J. Mol. Model.* **2009**, *15* (6), 723−729.
(12) Murray, J. S.; Lane, P.; Clark, T.; Riley, K. E.; Politzer, P. Sigma-holes, pi-holes and electrostatically-driven interactions. *J. Mol. Model.* **2012**, *18* (2), 541−548.
(13) Politzer, P.; Murray, J. S.; Clark, T. Halogen bonding and other sigma-hole interactions: a perspective. *Phys. Chem. Chem. Phys.* **2013**, *15* (27), 11178−11189.
(14) Riley, K. E.; Hobza, P. Investigations into the Nature of Halogen Bonding Including Symmetry Adapted Perturbation Theory Analyses. *J. Chem. Theory Comput.* **2008**, *4* (2), 232−242.
(15) Riley, K. E.; Murray, J. S.; Politzer, P.; Concha, M. C.; Hobza, P. Br−O Complexes as Probes of Factors Affecting Halogen Bonding: Interactions of Bromobenzenes and Bromopyrimidines with Acetone. *J. Chem. Theory Comput.* **2009**, *5* (1), 155−163.
(16) Lu, Y.; Shi, T.; Wang, Y.; Yang, H.; Yan, X.; Luo, X.; Jiang, H.; Zhu, W. Halogen Bonding, A Novel Interaction for Rational Drug Design? *J. Med. Chem.* **2009**, *52* (9), 2854−2862.
(17) Lu, Y.; Wang, Y.; Zhu, W. Nonbonding interactions of organic halogens in biological systems: implications for drug discovery and biomolecular design. *Phys. Chem. Chem. Phys.* **2010**, *12* (18), 4543−4551.
(18) Brahmkshatriya, P. S.; Dobes, P.; Fanfrlik, J.; Rezac, J.; Paruch, K.; Bronowska, A.; Lepsik, M.; Hobza, P. Quantum Mechanical Scoring: Structural and Energetic Insights into Cyclin-Dependent Kinase 2 Inhibition by Pyrazolo[1,5-a]pyrimidines. *Curr. Comput.-Aided Drug Des.* **2013**, *9* (1), 118−129.
(19) Dobes, P.; Rezac, J.; Fanfrlik, J.; Otyepka, M.; Hobza, P. Semiempirical Quantum Mechanical Method PM6-DH2X Describes the Geometry and Energetics of CK2-Inhibitor Complexes Involving Halogen Bonds Well, While the Empirical Potential Fails. *J. Phys. Chem. B* **2011**, *115* (26), 8581−8589.

(20) Jorgensen, W. L.; Schyman, P. Treatment of Halogen Bonding in the OPLS-AA Force Field: Application to Potent Anti-HIV Agents. *J. Chem. Theory Comput.* **2012**, *8* (10), 3895−3901.
(21) Kolar, M.; Hobza, P. On Extension of the Current Biomolecular Empirical Force Field for the Description of Halogen Bonds. *J. Chem. Theory Comput.* **2012**, *8* (4), 1325−1333.
(22) Voth, A. R.; Khuu, P.; Oishi, K.; Ho, P. S. Halogen bonds as orthogonal molecular interactions to hydrogen bonds. *Nat. Chem.* **2009**, *1* (1), 74−79.
(23) Politzer, P.; Murray, J. S.; Lane, P. sigma-Hole bonding and hydrogen bonding: Competitive interactions. *Int. J. Quantum Chem.* **2007**, *107* (15), 3046−3052.
(24) Shields, Z. P.; Murray, J. S.; Politzer, P. Directional tendencies of halogen and hydrogen bonds. *Int. J. Quantum Chem.* **2010**, *110* (15), 2823−2832.
(25) Politzer, P.; Murray, J. S.; Clark, T. Halogen bonding: an electrostatically-driven highly directional noncovalent interaction. *Phys. Chem. Chem. Phys.* **2010**, *12* (28), 7748−7757.
(26) Rezac, J.; Riley, K. E.; Hobza, P. Benchmark Calculations of Noncovalent Interactions of Halogenated Molecules. *J. Chem. Theory Comput.* **2012**, *8* (11), 4285−4292.
(27) Kozuch, S.; Martin, J. M. L. Halogen Bonds: Benchmarks and Theoretical Analysis. *J. Chem. Theory Comput.* **2013**, *9* (4), 1918−1931.
(28) Huber, K.; Brault, L.; Fedorov, O.; Gasser, C.; Filippakopoulos, P.; Bullock, A. N.; Fabbro, D.; Trappe, J.; Schwaller, J.; Knapp, S.; Bracher, F. 7,8-Dichloro-1-oxo-β-carbolines as a Versatile Scaffold for the Development of Potent and Selective Kinase Inhibitors with Unusual Binding Modes. *J. Med. Chem.* **2011**, *55* (1), 403−413.
(29) Fedorov, O.; Huber, K.; Eisenreich, A.; Filippakopoulos, P.; King, O.; Bullock, A. N.; Szklarczyk, D.; Jensen, L. J.; Fabbro, D.; Trappe, J.; Rauch, U.; Bracher, F.; Knapp, S. Specific CLK Inhibitors from a Novel Chemotype for Regulation of Alternative Splicing. *Chem. Biol.* **2011**, *18* (1), 67−76.
(30) Wilcken, R.; Liu, X.; Zimmermann, M. O.; Rutherford, T. J.; Fersht, A. R.; Joerger, A. C.; Boeckler, F. M. Halogen-enriched fragment libraries as leads for drug rescue of mutant p53. *J. Am. Chem. Soc.* **2012**, *134* (15), 6810−6818.
(31) Hardegger, L. A.; Kuhn, B.; Spinnler, B.; Anselm, L.; Ecabert, R.; Stihle, M.; Gsell, B.; Thoma, R.; Diez, J.; Benz, J.; Plancher, J.-M.; Hartmann, G.; Banner, D. W.; Haap, W.; Diederich, F. Systematic Investigation of Halogen Bonding in Protein−Ligand Interactions. *Angew. Chem., Int. Ed.* **2011**, *50* (1), 314−318.
(32) Hardegger, L. A.; Kuhn, B.; Spinnler, B.; Anselm, L.; Ecabert, R.; Stihle, M.; Gsell, B.; Thoma, R.; Diez, J.; Benz, J.; Plancher, J.-M.; Hartmann, G.; Isshiki, Y.; Morikami, K.; Shimma, N.; Haap, W.; Banner, D. W.; Diederich, F. Halogen Bonding at the Active Sites of Human Cathepsin L and MEK1 Kinase: Efficient Interactions in Different Environments. *ChemMedChem* **2011**, *6* (11), 2048−2054.
(33) Lam, P. Y. S.; Clark, C. G.; Smallwood, A. M.; Alexander, R. S., Structure-based drug design utilizing halogen bonding: Factor Xa inhibitors. In *238th ACS National Meeting*, Washington, D.C., United States, Aug 16−20, 2009.
(34) Njoroge, F. G.; Vibulbhan, B.; Pinto, P.; Strickland, C.; Bishop, W. R.; Nomeir, A.; Girijavallabhan, V. Enhanced FTase activity achieved via piperazine interaction with catalytic zinc. *Bioorg. Med. Chem. Lett.* **2006**, *16* (4), 984−988.
(35) Strickland, C. L.; Weber, P. C.; Windsor, W. T.; Wu, Z.; Le, H. V.; Albanese, M. M.; Alvarez, C. S.; Cesarz, D.; del Rosario, J.; Deskus, J.; Mallams, A. K.; Njoroge, F. G.; Piwinski, J. J.; Remiszewski, S.; Rossman, R. R.; Taveras, A. G.; Vibulbhan, B.; Doll, R. J.; Girijavallabhan, V. M.; Ganguly, A. K. Tricyclic farnesyl protein transferase inhibitors: crystallographic and calorimetric studies of structure-activity relationships. *J. Med. Chem.* **1999**, *42* (12), 2125−2135.
(36) Grimme, S. Semiempirical GGA-type density functional constructed with a long-range dispersion correction. *J. Comput. Chem.* **2006**, *27* (15), 1787−1799.
(37) Halkier, A.; Helgaker, T.; Jørgensen, P.; Klopper, W.; Koch, H.; Olsen, J.; Wilson, A. K. Basis-set convergence in correlated calculations on Ne, N2, and H2O. *Chem. Phys. Lett.* **1998**, *286* (3−4), 243−252.
(38) Klamt, A.; Schüürmann, G. Cosmo - a New Approach to Dielectric Screening in Solvents with Explicit Expressions for the Screening Energy and Its Gradient. *J. Chem. Soc., Perkin Trans. 2* **1993**, *5*, 799−805.
(39) Klamt, A.; Eckert, F. COSMO-RS: a novel and efficient method for the a priori prediction of thermophysical data of liquids. *Fluid Phase Equilib.* **2000**, *172* (1), 43−72.
(40) Riley, K. E.; Murray, J. S.; Fanfrlik, J.; Rezac, J.; Sola, R. J.; Concha, M. C.; Ramos, F. M.; Politzer, P. Halogen bond tunability II: the varying roles of electrostatic and dispersion contributions to attraction in halogen bonds. *J. Mol. Model.* **2012**, DOI: 10.1007/s00894-012-1428-x.
(41) Hobza, P.; Riley, K. The Relative Roles of Electrostatics and Dispersion in the Stabilization of Halogen Bonds. *Phys. Chem. Chem. Phys.* **2013**, *15* (41), 17742−17751.
(42) Weber, J.; Achenbach, J.; Moser, D.; Proschak, E. VAMMPIRE: a matched molecular pairs database for structure-based drug design and optimization. *J. Med. Chem.* **2013**, *56* (12), 5203−5207.
(43) Ahlrichs, R.; Bar, M.; Haser, M.; Horn, H.; Kolmel, C. Electronic-Structure Calculations on Workstation Computers - the Program System Turbomole. *Chem. Phys. Lett.* **1989**, *162* (3), 165−169.
(44) *TURBOMOLE*, V6.2 2010; TURBOMOLE GmbH: Karlsruhe, Germany, 2010.
(45) Weigend, F.; Ahlrichs, R. Balanced basis sets of split valence, triple zeta valence and quadruple zeta valence quality for H to Rn: Design and assessment of accuracy. *Phys. Chem. Chem. Phys.* **2005**, *7* (18), 3297−3305.
(46) Weigend, F.; Haser, M.; Patzelt, H.; Ahlrichs, R. RI-MP2: optimized auxiliary basis sets and demonstration of efficiency. *Chem. Phys. Lett.* **1998**, *294* (1−3), 143−152.
(47) Feyereisen, M.; Fitzgerald, G.; Komornicki, A. Use of Approximate Integrals in Abinitio Theory - an Application in Mp2 Energy Calculations. *Chem. Phys. Lett.* **1993**, *208* (5−6), 359−363.
(48) Hattig, C. Optimization of auxiliary basis sets for RI-MP2 and RI-CC2 calculations: Core-valence and quintuple-[small zeta] basis sets for H to Ar and QZVPP basis sets for Li to Kr. *Phys. Chem. Chem. Phys.* **2005**, *7* (1), 59−66.
(49) Boys, S. F.; Bernardi, F. The calculation of small molecular interactions by the differences of separate total energies. Some procedures with reduced errors. *Mol. Phys.* **1970**, *19*, 553−566.
(50) Baerends, E. J.; Ellis, D. E.; Ros, P. Self-consistent molecular Hartree—Fock—Slater calculations I. The computational procedure. *Chem. Phys.* **1973**, *2* (1), 41−51.
(51) Dunlap, B. I.; Connolly, J. W. D.; Sabin, J. R. On some approximations in applications of X alpha theory. *J. Chem. Phys.* **1979**, *71* (8), 3396−3402.
(52) Weigend, F. Accurate Coulomb-fitting basis sets for H to Rn. *Phys. Chem. Chem. Phys.* **2006**, *8* (9), 1057−1065.
(53) Becke, A. D. Density-functional exchange-energy approximation with correct asymptotic behavior. *Phys. Rev. A: At. Mol. Opt. Phys.* **1988**, *38* (6), 3098−3100.
(54) Perdew, J. P. Density-functional approximation for the correlation energy of the inhomogeneous electron gas. *Phys. Rev. B: Condens. Matter Mater. Phys.* **1986**, *33* (12), 8822−8824.
(55) Lee, C.; Yang, W.; Parr, R. G. Development of the Colle-Salvetti correlation-energy formula into a functional of the electron density. *Phys. Rev. B: Condens. Matter Mater. Phys.* **1988**, *37* (2), 785−789.
(56) Staroverov, V. N.; Scuseria, G. E.; Tao, J.; Perdew, J. P. Comparative assessment of a new nonempirical density functional: Molecules and hydrogen-bonded complexes. *J. Chem. Phys.* **2003**, *119* (23), 12129−12137.
(57) Becke, A. D. Density-functional thermochemistry. III. The role of exact exchange. *J. Chem. Phys.* **1993**, *98* (7), 5648−5652.

(58) Dunning, J. T. H. Gaussian basis sets for use in correlated molecular calculations. I. The atoms boron through neon and hydrogen. *J. Chem. Phys.* **1989**, *90* (2), 1007−1023.
(59) Woon, D. E.; Dunning, T. H., Jr. Gaussian Basis Sets for Use in Correlated Molecular Calculations. III. The second row atoms, Al-Ar. *J. Chem. Phys.* **1993**, *98*, 1358−1371.
(60) Peterson, K. A.; Shepler, B. C.; Figgen, D.; Stoll, H. On the Spectroscopic and Thermochemical Properties of ClO, BrO, IO, and Their Anions. *J. Phys. Chem. A* **2006**, *110* (51), 13877−13883.
(61) Weigend, F.; Kohn, A.; Hattig, C. Efficient use of the correlation consistent basis sets in resolution of the identity MP2 calculations. *J. Chem. Phys.* **2002**, *116* (8), 3175−3183.
(62) Werner, H.-J.; Knowles, P. J.; Lindh, R.; Manby, F. R.; Schütz, M.; Celani, P.; Korona, T.; Rauhut, G.; Amos, R. D.; Bernhardsson, A.; Berning, A.; Cooper, D. L.; Deegan, M. J. O.; Dobbyn, A. J.; Eckert, F.; Hampel, C.; Hetzer, G.; Lloyd, A. W.; McNicholas, S. J.; Meyer, W.; Mura, M. E.; Nicklass, A.; Palmieri, P.; Pitzer, R.; Schumann, U.; Stoll, H.; Stone, A. J.; Tarroni, R.; Thorsteinsson, T. *MOLPRO*, 2006.1, a package of *ab initio* programs; see http://www.molpro.net.
(63) Hobza, P.; Šponer, J. Toward True DNA Base-Stacking Energies: MP2, CCSD(T), and Complete Basis Set Calculations. *J. Am. Chem. Soc.* **2002**, *124* (39), 11802−11808.
(64) Jurecka, P.; Sponer, J.; Cerny, J.; Hobza, P. Benchmark database of accurate (MP2 and CCSD(T) complete basis set limit) interaction energies of small model complexes, DNA base pairs, and amino acid pairs. *Phys. Chem. Chem. Phys.* **2006**, *8* (17), 1985−1993.
(65) Delano, W. L. *The PyMOL Molecular Graphics System*; DeLano Scientific LLC: Palo Alto, CA, USA, 2008.
(66) Brickmann, J.; Exner, T. E.; Keil, M.; Marhofer, R. J. Molecular graphics - Trends and perspectives. *J. Mol. Model.* **2000**, *6* (2), 328−340.
(67) Brickmann, J.; Exner, T. E.; Gimmler, J.; Lautenschläger, P.; Heiden, W.; Moeckel, G.; Zahn, D. *MOLCAD II*, V1.4; MOLCAD GmbH: Darmstadt, Germany; http://www.molcad.de, 2013.